Recent developments on wall-bounded turbulence

Javier Jiménez

Abstract.   The study of turbulence near walls has experienced a renaissance in the last decade, in part because of the availability of high-quality numerical simulations. The viscous and buffer layers over smooth walls are now fairly well understood. They are essentially independent of the outer flow, and there is a family of numerically-exact nonlinear structures that predict well many of the best-known characteristics of the wall layer, such as the intensity and the spectra of the velocity fluctuations, and the dimensions of the dominant structures. Much of this progress was made possible by the increase in computer power that made the kinematic simulations of the late 1980s cheap enough to undertake conceptual dynamical experiments. We are today at the early stages of simulating the logarithmic layer. A kinematic picture of the various processes present in that part of the flow is beginning to emerge, and it is leading to a rough dynamical understanding. Some of it, surprisingly, in terms of linear models. Many processes mimic those in the buffer layer, but in an averaged LES sense, rather than applied to individual structures. The paper discusses the present status of our understanding of this region, and possible future developments.

Desarrollos recientes sobre la turbulencia de pared

Resumen.   El estudio de la turbulencia parietal ha renacido en la última década, debido en parte a la aparición de simulaciones numéricas de alta calidad. Las capas viscosas y tampón cercanas a la pared se entienden hoy día bastante bien. Esencialmente son independientes del flujo exterior, y existe una familia de soluciones no lineales a la ecuaciones del flujo, numéricamente exactas, que predicen adecuadamente muchas de las características más conocidas de esta capa parietal, tales como la intensidad y los espectros de las fluctuaciones de velocidad, o las dimensiones de las estructuras dominantes. Una gran parte de estos avances fue posible gracias al aumento de la potencia de los ordenadores, que hizo que las simulaciones cinemáticas de los años 1980 se abarataran hasta permitir experimentos dinámicos conceptuales unos años más tarde. Hoy día estamos iniciando las primeras simulaciones de la capa logarítmica. Esto nos ha proporcionado un esbozo cinemático de los distintos procesos de esa región del flujo, y una primera aproximación a su dinámica; sorprendentemente, usando en algunos casos modelos lineales. Muchos de los procesos recuerdan a los de la capa tampón, pero en un sentido promediado, en vez de aplicados a estructuras individuales. Este artículo discute el estado actual de nuestra comprensión de esta parte del flujo, y los probables desarrollos futuros.

1   Introduction

Any paper on turbulence in a mathematical journal has to start with a disclaimer, because it deals with chaotic solutions to the Navier–Stokes equations, for which existence and uniqueness results are mostly

unavailable. We will restrict ourselves here to the incompressible case, for which the equations of motion are,

$$\partial_t \mathbf{u} + \mathbf{u}\nabla\mathbf{u} + \rho^{-1}\,\nabla p = \nu\nabla^2\mathbf{u}, \tag{1}$$

$$\nabla \cdot \mathbf{u} = 0, \tag{2}$$

where $\mathbf{u}$ is the vector velocity, p is the pressure, ρ is the fluid density, assumed constant, and ν the kinematic viscosity.

Even in the absence of proof, there is overwhelming experimental and theoretical evidence that the behaviour of fluids is well described by (1)–(2) for scales larger than the mean free path between molecular collisions, λ_g. The smallest active scale of a turbulent flow is, at least in the mean, the Kolmogorov viscous scale η [53], which is at least of order $O(Re^{1/4}\lambda_g)$ for a gas. The Reynolds number $Re = u'L_\varepsilon/\nu$ is given in terms of the root-mean-square intensity of the velocity fluctuations u', and of the integral scale of the largest eddies L_ε. It measures the scale ratio between the largest and the smallest turbulent scales, and it is typically of the order of thousands, or millions. It is then always true that $\eta \gg \lambda_g$, and that turbulent flows are described almost everywhere by (1)–(2). There are theoretical reasons to suspect that scales of the order of λ_g may appear locally and intermittently [28], but the same arguments show that they should not influence any low-order integral quantities such as the energy or the enstrophy. This is confirmed by experiments.

We will therefore not worry here about existence problems, or even about the question of turbulence in general. The paper deals with the features that distinguish sheared turbulence in the neighbourhood of walls from free shear flows, and we will see that those differences are mostly restricted to relatively large structures, for which intermittency has little influence.

Wall-bounded turbulence includes pipes, channels and boundary layers. We will restrict ourselves to cases with little or no longitudinal pressure gradients, since otherwise the flow tends to separate, and to resemble the free shear case. It was in attached wall-bounded flows where turbulence was first studied scientifically [16, 12], but they remain to this day worse understood than homogeneous or free-shear flows. That is in part because what is sought in both cases is different. Turbulence is a multiscale phenomenon. Energy resides in the largest eddies, but it cannot be dissipated until it is transferred to the smaller scales where viscosity can act. The classical conceptual framework for that process is the self-similar cascade proposed in [46], which basically assumes that the transfer is local in scale space, with no significant interactions between eddies of very different sizes. From that model, and from energy conservation arguments, Kolmogorov [35] derived how energy is distributed among the inviscid eddies in the 'inertial' range of scales of statistically homogeneous flows. He also computed the viscous scale that we have mentioned above, where the energy is finally dissipated, and where the inertial cascade ends. The resulting energy spectrum, although now recognized as only an approximation, describes well the experimental observations, not only for isotropic turbulence, but also for small-scale turbulence in general. A sketch can be found in figure 1(a).

Isotropic theory gives no indication of how energy is fed into the turbulent cascade. In shear flows, the energy source is the gradient of the mean velocity. The mechanism is the interaction between that gradient and the average momentum fluxes carried by the velocity fluctuations [53]. In free shear flows, such as jets or mixing layers, this leads to a large-scale instability of the mean velocity profile [9], and to large-scale eddies with sizes of the order of the flow thickness. Those 'integral' scales contain most of the energy. The subsequent transfer to the smaller eddies is thought to be essentially similar to the isotropic case.

The mean velocity profiles of wall-bounded flows, such as pipes or boundary layers, are not unstable in the same way as the free shear cases, although we will see later that the energy of linear perturbations can still grow. Wall-bounded turbulence is consequently a weaker phenomenon. While the velocity fluctuations in a jet can easily reach 15-20% of the mean velocity differences, they rarely exceed 5% in a boundary layer. Wall-bounded flows are however of huge technological importance. Probably half of the energy being spent worldwide to move fluids through pipes and canals, or to move vehicles through air or through water, is dissipated by turbulence in the immediate vicinity of the wall.

Wall-bounded flows are also interesting because they force us to face squarely the role of inhomogeneity. This can be seen in figure 1(b) which is the equivalent of figure 1(a) for a wall-bounded turbulent flow.
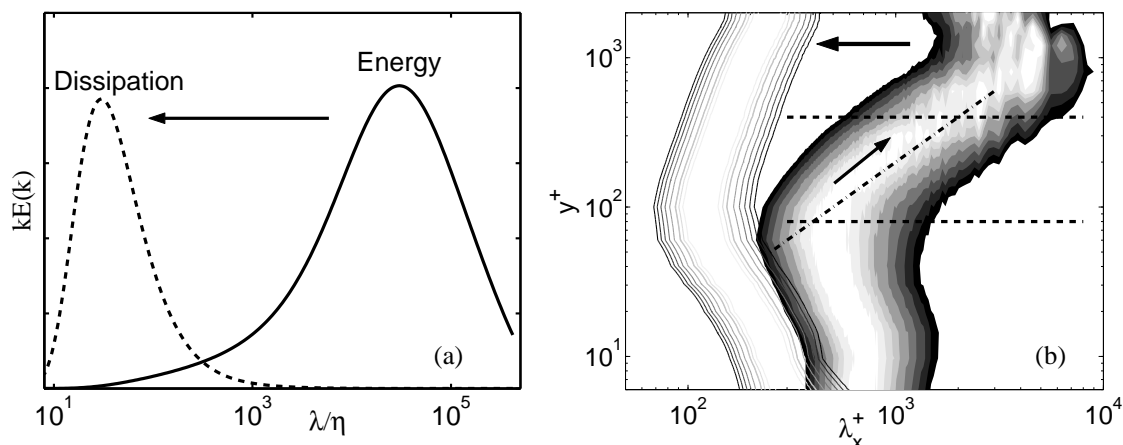
Figure 1. Spectral energy density, $kE(k)$. (a) In isotropic turbulence, as a function of the isotropic wavelength $\lambda = 2\pi/|k|$. (b) In a numerical turbulent channel [18] with half-width $h^+ = 2000$, plotted as a function of the streamwise wavelength λ_x, and of the wall distance y. The shaded contours are the density of the kinetic energy of the velocity fluctuations, $k_x E_{\mathbf{uu}}(k_x)$. The lines are the spectral density of the surrogate dissipation, $\nu k_x E_{\omega\omega}(k_x)$, where ω are the vorticity fluctuations. At each y the lowest contour is 0.86 times the local maximum. The horizontal lines are $y^+ = 80$ and $y/h = 0.2$, and represent conventional limits for the logarithmic layer. The diagonal is $\lambda_x = 5y$. The arrows indicate the implied cascades.

Each horizontal section of this figure is equivalent to the spectra in figure 1(a). The energy is again at large scales, while the dissipative eddies are smaller. In this case, however, the size of the energy-containing eddies changes with the distance to the wall, and so does the range of scales over which the energy has to cascade. The eddy sizes containing most of the energy at one wall distance are in the midst of the inertial cascade when they are observed farther away from the wall. The Reynolds number, defined as the scale disparity between energy and dissipation at some given location, also changes with wall distance. The main emphasis in wall turbulence is not on the inertial energy cascade, but on the interplay between different scales at different distances from the wall.

Models for wall-bounded turbulence also have to deal with spatial fluxes that are not present in the homogeneous case. The most important ones are those of momentum. Consider a turbulent channel, driven by a pressure gradient between infinite parallel planes, and decompose the flow quantities into mean values and fluctuations with respect to those means. Denote by U, V and W the mean velocities along the streamwise, wall-normal and spanwise directions, x, y and z, and the corresponding fluctuations by lower-case letters. Using streamwise and spanwise homogeneity, and assuming that the averaged velocities are stationary, the mean streamwise momentum equation is

$$\partial_y \langle uv \rangle + \rho^{-1} \partial_x P = \nu \partial_{yy} U, \tag{3}$$

where the average $\langle \cdot \rangle$ is conceptually defined over many equivalent independent experiments. Streamwise momentum is fed into the channel by the mean pressure gradient, $\partial_x P$, which acts over its whole cross section. It is removed only at the wall, by viscous friction. Momentum has to flow from the centre to the wall, carried that way by the averaged momentum flux of the fluctuations, $-\langle uv \rangle$, which is called the kinematic Reynolds stress. Reynolds stresses reside in eddies of roughly the same scales as the energy, and it is clear from figure 1(b) that the sizes of the stress-carrying eddies change as a function of the wall distance by as much as the scale of the energy across the inertial cascade. This implies that momentum is transferred in wall-bounded turbulence by an extra spatial cascade. Momentum transport is present in all shear flows, but the multiscale spatial cascade is characteristic of very inhomogeneous situations, such as

wall turbulence, and complicates the problem considerably.

This paper is both a review and a prospective. In the next section we outline the classical theory of wall-bounded flows, and define the different flow regions. In section 3 we review the current structural understanding of the near-wall viscous layers, including recent work on equilibrium exact solutions to the equations of motions, and how they are related to turbulence. This is the review part of the paper, and it can be considered as relatively well established. The remaining sections deal with the outer layers, about which less is known, and it is mostly a road map of what, in the opinion of the author, would need to be done in the next few years to complete our knowledge of those regions.

2   The classical theory of wall-bounded turbulence

The wall-normal variation of the length of the energy cascade divides the flow into several distinct regions. Wall-bounded turbulence over smooth walls can be described by two sets of scaling parameters [53]. Viscosity is important near the wall, and the units for length and velocity in that region are constructed with the kinematic viscosity ν and with the friction velocity $u_\tau = (\tau_w/\rho)^{1/2}$, which is based on the shear stress at the wall τ_w, and on the fluid density ρ. Magnitudes expressed in those 'wall units' are denoted by $^+$ superscripts. There is no scale disparity in this region, as seen in figure 1(b), because most large eddies are excluded by the presence of the impermeable wall. The energy and the dissipation are at similar sizes. If y is the distance to the wall, y^+ is a Reynolds number for the size of the structures, and it is never large within the viscous layer, which is typically defined at most as $y^+ \lesssim 150$ [41]. It is conventionally divided into a viscous sublayer, $y^+ \lesssim 5$, where viscosity is dominant, and a 'buffer' layer in which both viscosity and inertial effects should be taken into account.

Away from the wall the velocity also scales with u_τ, because the momentum equation requires that the Reynolds stress, $-\langle uv \rangle$, can only change slowly with y to compensate for the pressure gradient. This uniform velocity scale is the extra constraint introduced in wall-bounded flows by the momentum transfer. The length scale in the region far from the wall is the flow thickness h. In most of the examples in this paper, h will be the semi-channel height, from the wall to the central plane. Between the inner and the outer regions there is an intermediate layer where the only available length scale is the wall distance y.

Both the constant velocity scale across the intermediate region, and the absence of a length scale other than y, are only approximations. It will be seen below that large-scale eddies of size $O(h)$ penetrate to the wall, and that the velocity does not scale strictly with u_τ even in the viscous sublayer. However, if those approximation are accepted, it follows from symmetry arguments that the mean velocity in this 'logarithmic' layer is

$$U^+ = \kappa^{-1} \log y^+ + A. \tag{4}$$

This forms agrees well with experimental evidence, with an approximately universal Kármán constant, $\kappa \approx 0.4$, but the theoretical argument has been repeatedly challenged, and a short critical discussion will be included in section 4.1.

Equation (4) does not extend to the wall, and the intercept constant A depends on the details of the viscous near-wall region. For smooth walls, $A \approx 5$.

The viscous, buffer, and logarithmic layers are the most characteristic features of wall-bounded flows, and they constitute the main difference between those flows and other types of turbulence.

The viscous and buffer layers are extremely important for the flow as a whole. The ratio between the inner and the outer length scales is the friction Reynolds number, h^+, which ranges from 200 for barely turbulent flows, to 5×10^5 for large water pipes. In the latter, the near-wall layer is only about 3×10^{-4} times the pipe radius, but it follows from (4) that, even in that case, 40% of the velocity drop takes place below $y^+ = 50$. Because there is relatively little energy transfer among layers, except in the viscous region, those percentages also apply to where the energy is dissipated. Turbulence is characterized by the expulsion towards the small scales of the energy dissipation, away from the large energy-containing eddies. In the limit of infinite Reynolds number, this is believed to lead to a non-differentiable velocity field. In wall-bounded flows that separation occurs not only in the scale space for the velocity fluctuations, but also in the

shape of the mean velocity profile for the momentum transfer. The singularities are expelled both from the large scales, and from the centre of the flow towards the logarithmic layers near the walls.

Because of this 'singular' nature, the near-wall layer is not only important for the rest of the flow, but it is also largely independent from it. That was for example shown by numerical experiments in [26], where the outer flow was artificially removed above a certain wall distance δ. The near-wall dynamics was essentially unaffected as long as $\delta^+ \gtrsim 60$.

The near-wall layer is relatively easy to simulate numerically, because the local Reynolds numbers are low, but it is difficult to study experimentally, because it is usually very thin in laboratory flows. Its modern study began experimentally in the 1970's [31, 38], but it got its strongest impulse with the advent of high-quality direct numerical simulations in the late 1980's and in the 1990's [32]. We will see below that it is one of the turbulent systems about which most is known.

The logarithmic law is located just above the near-wall layer, and it is also unique to wall turbulence. Most of the velocity difference that does not reside in the near-wall region is concentrated in the logarithmic layer, which extends experimentally up to $y \approx 0.2h$ (figure 1b). It follows from (4) that the velocity difference above the logarithmic layer is only 20% of the total when $h^+ = 200$, and that it decreases logarithmically as the Reynolds number increases. In the limit of infinite Reynolds number, all the velocity drop is in the logarithmic layer.

The logarithmic layer is an intrinsically high-Reynolds number phenomenon. Its existence requires at least that its upper limit should be above the lower one, so that $0.2h^+ \gtrsim 150$, and $h^+ \gtrsim 750$. The local Reynolds numbers y^+ of the eddies are also never too low. The logarithmic layer has been studied experimentally for a long time, but numerical simulations with even an incipient logarithmic region have only recently become available [4, 18, 14]. It is much worse understood than the viscous layers.

3 Models for the buffer layer

The region below $y^+ \approx 100$ is dominated by coherent streaks of the streamwise velocity and by quasi-streamwise vortices. The former are an irregular array of long ($x^+ \approx 1000$) sinuous alternating streamwise jets superimposed on the mean shear, with an average spanwise separation of the order of $z^+ \approx 100$ [51]. The quasi-streamwise vortices are slightly tilted away from the wall, and stay in the near-wall region only for $x^+ \approx 200$. Several vortices are associated with each streak [24], with a longitudinal spacing of the order of $x^+ \approx 400$. Most of them merge into disorganized vorticity outside the immediate neighbourhood of the wall [47].

It was proposed soon after they were discovered that streaks and vortices were involved in a regeneration cycle in which the vortices were the results of an instability of the streaks [52], while the streaks were caused by the advection of the mean velocity gradient by the vortices [7, 31]. Both processes have been documented and sharpened by numerical experiments. For example, disturbing the streaks inhibits the formation of the vortices, but only if it is done between $y^+ \approx 10$ and $y^+ \approx 60$ [26], suggesting that it is predominantly between those two levels that the regeneration cycle works. There is a substantial body of numerical [17, 57, 49] and analytic [42, 29] work on the linear instability of model streaks. It shows that streaks are unstable to sinuous perturbations associated with inflection points of the distorted velocity profile, whose eigenfunctions correspond well with the shape and location of the observed vortices. The model implied by these instabilities is a time-dependent cycle in which streaks and vortices are created, grow, generate each other, and eventually decay. Reference [26] discusses unsteady models of this type, and gives additional references.

Although the flow in the buffer layer is clearly chaotic, the chaos is not required to explain the turbulence statistics. Simulations in which the flow is substituted by an ordered 'crystal' of identical 'minimal' sets of structures [24] reproduce the correct statistics (figure 2). In a further simplification, that occurred at roughly the same time as the previous one, nonlinear equilibrium solutions of the three-dimensional Navier–Stokes equations were obtained numerically, with characteristics that suggested that they could be useful in a dynamical description of the near-wall region [39]. Other such solutions were soon found for plane Couette
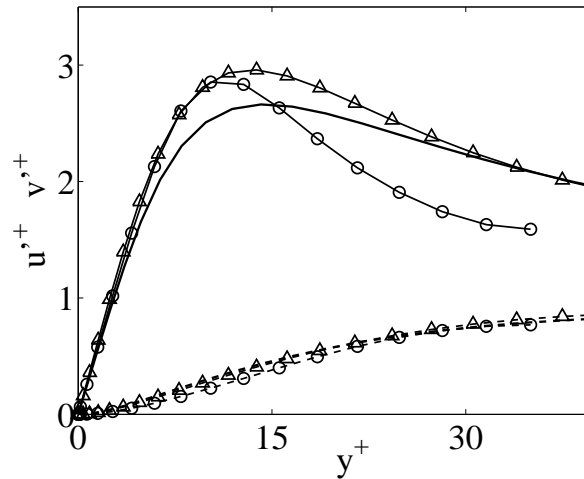
Figure 2. Profiles of the root-mean-square velocity fluctuations. Simple lines are a full channel with $h^+ = 180$ [32]; —△—, a minimal channel with $h^+ = 180$ [24]; —○—, a permanent-wave autonomous solution [27]. ——, streamwise velocity; - - - -, wall-normal velocity.

flow [39, 60], plane Poiseuille flow [54, 59, 60], and for an autonomous wall flow [27]. All those solutions look qualitatively similar [58, 29], and take the form of a wavy low-velocity streak flanked by a pair of staggered quasi-streamwise vortices of alternating signs, closely resembling the spatially-coherent objects educed from the near-wall region of true turbulence.

In those cases in which the stability of the equilibrium solutions has been investigated, they have been found to be saddles in phase space, with few unstable directions. The flow could therefore spend a substantial fraction of its lifetime in their neighbourhood, because its orbit would move slowly in the neighbourhood of the fixed point. Exact limit cycles, and heteroclinic orbits based on these fixed points, have been found numerically [30, 55], and several reduced dynamical models of the near-wall region have been formulated in terms of low-dimensional projections of such solutions [6, 50, 57].

The fixed-point and limit-cycle solutions found by different authors were recently reviewed and extended in [23]. It turns out that they can be classified into 'upper' and 'lower' branches in terms of their mean wall shear, and that both branches have very different profiles of their fluctuation intensities. The 'upper' solutions have relatively weak sinuous streaks flanked by strong vortices. They consequently have relatively weak root-mean-square streamwise-velocity fluctuations, and strong wall-normal ones, at least when compared to those in the lower branch. Their mean and fluctuation intensity profiles are reminiscent of experimental turbulence [27, 60], as shown in figure 2, and so are several other properties. For example, the range of spanwise wavelengths in which the nonlinear solutions exist is always in the neighbourhood of the observed spacing of the streaks of the sublayer [23]. 'Lower' solutions have stronger and essentially straight streaks, and much weaker vortices. Their statistics are very different from turbulence.

The near-wall statistics of full turbulent flows, when compiled over scales corresponding to a single streak and to a single vortex pair, are independent of the Reynolds number, and agree reasonably well with those of the fixed points, although there is a noticeable contribution from unsteady bursting [23]. When they are compiled over much larger boxes, however, the intensity of the fluctuations does not scale well in wall units, even very near the wall [13]. That effect is due to large outer-flow velocity fluctuations reaching the wall, and it is unrelated to the structures being considered in this section.

This is shown in figure 3, which contains two-dimensional spectral energy densities of the streamwise velocity, $k_x k_z E_{uu}(k_x, k_z)$ in the buffer layer, displayed as functions of the streamwise and spanwise wavelengths. The three spectra in the figure correspond to turbulent channels at different Reynolds numbers. They differ from each other almost exclusively in the long and wide structures represented in the upper-
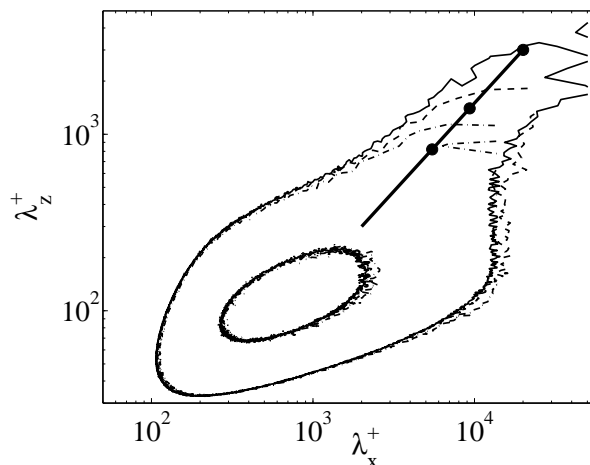
Figure 3. Two-dimensional spectral energy density of the streamwise velocity in the near-wall region $(y^+ = 15)$, in terms of the streamwise and spanwise wavelengths. Numerical channels [2, 4, 18]. —·— , $h^+ = 547$; ---- , 934; ——— , 2003. Spectra are normalized in wall units, and the two contours for each spectrum are 0.125 and 0.625 times the maximum of the spectrum for the highest Reynolds number. The heavy straight line is $\lambda_z = 0.15\lambda_x$, and the heavy dots are $\lambda_x = 10h$ for the three cases.

right corner of the spectrum, whose sizes are of the order of $\lambda_x \times \lambda_z = 10h \times h$. Those spectra are fairly well understood [2, 22, 18]. The lower-left corner contains the structures discussed in this section, which are very approximately universal and local to the near-wall layer. The larger structures in the upper edge of the spectra, and specially those in the top-right corner, extend into the logarithmic layer, scale in outer units, and correspond approximately to the 'attached eddies' that were proposed long ago by Townsend [56].

4 The logarithmic layer

We noted in section 2 that the logarithmic layer is expensive to compute. The first simulations with an appreciable logarithmic region have only recently appeared, but even in them the relevant range of wall distances is short. In figure 1(b), for example, $h^+ = 2000$, and the upper and lower logarithmic limits are approximately $y^+ = 400$ and $y^+ = 150$. Even so, those simulations, as well as simultaneous advances in experimental methods, have greatly improved our understanding of the kinematics of the structures in this region, and are beginning to hint at their dynamics.

Before considering those results, it is important to remark that the meaning of the word 'model' is probably always going to be different in the logarithmic and in the buffer layer. Near the wall, the local Reynolds numbers are low, and the structures are smooth and essentially analytic. It is then possible to speak of 'objects', and to write differential equations for their behaviour. Above the buffer layer, both things are harder to do. In the logarithmic layer, the integral scale is $L_\varepsilon \approx y$, the r.m.s. velocity fluctuations are $O(u_\tau)$, and the turbulent Reynolds number is $Re = O(y^+)$. The definition of the outer layer, $y^+ \gg 1$, implies that most of its structures have large internal Reynolds numbers, and that they are most probably turbulent themselves. There is presumably a cascade connecting the energy-containing structures with the dissipative scales, and their velocity fields can be expected to have nontrivial algebraic spectra and non-smooth geometries. Such objects 'have no shape', and can only be described statistically. They are 'eddies', rather than 'vortices', because turbulent vorticity is always at the viscous Kolmogorov length scale η, separated from the energy-containing eddies by a scale ratio $L_\varepsilon/\eta \approx Re^{3/4}$. An example of such an object is given below in figure 5.

While the models discussed above for the buffer layer are in the realm of direct numerical simulations (DNS), and of classically identifiable structures, in the outer layers we are in the domain of large-eddy simulations (LES), and of statistical modelling, in the sense that we cannot probably find simple structures including all the scales of the flow. The most that we can expect is a simple description of the statistics of the larger scales, coupled to a stochastic model for the turbulent cascade 'underneath'. This of course does not mean that the logarithmic layer can not be DNSed, and this author firmly believes that such direct simulations will be required before this part of the flow is understood, but the tools of choice are different. We have seen above that DNS has been the driving force behind the revival of turbulence research in the past few decades and that, for the buffer layer, it has also been the predominant technique. Experiments are difficult very near the wall, while simulations are relatively simple. Experimental results in that region are few, and, whenever a disagreement is found between numerics and experiments, it can probably be assumed that the simulations are right. The same is not true in the logarithmic layer. It is still true that DNS provides an unprecedented level of detail on the flow, and that it allows conceptual experiments that are difficult to carry out in a wind tunnel, but outer-layer experiments are plentiful and reliable. Any model of those regions has to reconcile the results of both techniques.

Perhaps the first new information provided by the numerics on the logarithmic layer was spectral. It had been found experimentally that there are very large scales in the outer regions of turbulent boundary layers [20, 33], and DNS provided information about their two-dimensional spectra, and about their wall-normal correlations [2, 4]. The longest scales are associated with the streamwise velocity component u. Its spectral density in the logarithmic layer has an elongated shape along the line $\lambda_z^2 = y\lambda_x$, while the two other velocity components are more isotropic (see figure 4).

When three-dimensional flow fields eventually became available, it was found that there is a self-similar hierarchy of compact ejections extending from the buffer layer into the outer flow, within which the coarse-grained dissipation is more intense than elsewhere [5]. They correspond to the isotropic spectra of v in figure 4(a). When the flow is conditionally averaged around them, these ejections are seen to be associated with extremely long, conical, low-velocity regions in the logarithmic layer [5]. The intersection of those cones with the plane defined by a given wall distance is parabolic, and explains the quadratic behaviour of the spectrum of u. These structures are not only statistical constructs. Individual cones are observed as low-momentum 'ramps' in streamwise sections of instantaneous flow fields [36], and one of them can be seen in the streamwise velocity isosurface in figure 5.

When the cones reach heights of the order of the flow thickness, they stop growing, and become long cylindrical 'streaks', similar to those of the sublayer, but with spanwise scales of $2 - 3h$. They are fully turbulent objects. Neither in simulations nor in experiments has it been possible to determine a maximum length for those 'global modes'. They cross numerical boxes of length $25h$ (see figures 4 and 5), and, in experiments, they are of the same order as the wind-tunnel dimensions [19]. The overall arrangement of the ejections and cones is reminiscent of the association of vortices and streaks in the buffer layer, but at a much larger scale.

The wall-normal dimension of these streaks is of the order of the flow thickness, and they span the distance from the central plane to the wall [2, 4]. Their near-wall footprints are seen in the spectra of the buffer layer as the 'tails' in figure 3, and account [18] for the experimentally-observed Reynolds number dependence of the intensity of the near-wall velocity fluctuations [13]. Less easily explained is the more controversial Reynolds-number dependence of u'^+ in the logarithmic layer, initially also observed in [13], but there is also evidence of its association with the large-scale streaks. The dependence disappears when the spectral energy associated with the global streaks is removed (see figure 6). That would imply that the velocity fluctuations in the large streaks do not scale with u_τ, which is indeed suggested by the analysis of both experimental and numerical data [4]. That issue can however be considered as open.

Since we saw above that the sublayer streaks originate from the advection of the mean shear by cross-stream perturbations, which is a linear process, there is some hope that a linear model could also capture the formation of the outer-layer streaks. The mean velocity profile of turbulent channels is linearly stable [45], but it has been known for some time that even stable flows can lead to large transient energy amplifications, because the evolution operator of the linearized Navier–Stokes equations is not self-adjoint [15, 10, 43].
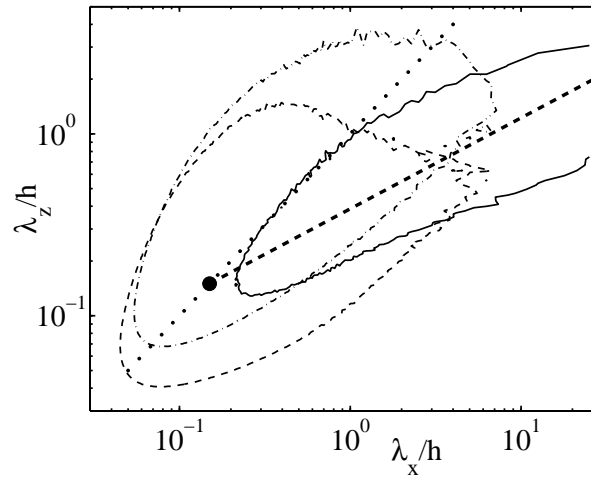
194

Figure 4. Two-dimensional spectral densities of the streamwise and transverse velocities in the logarithmic region, $y/h = 0.15$, in terms of the streamwise and spanwise wavelengths. Numerical channel with $h^+ = 2000$ [18]. ——— , $k_x k_z E_{uu}$; - - - - , $k_x k_z E_{vv}$; —·— , $k_x k_z E_{ww}$. The contour for each spectra is 0.25 times its maximum. The dashed straight line is $\lambda_z = (y\lambda_x)^{1/2}$. The dotted one is $\lambda_z = \lambda_x$. The heavy dot is $\lambda_z = \lambda_x = y$.
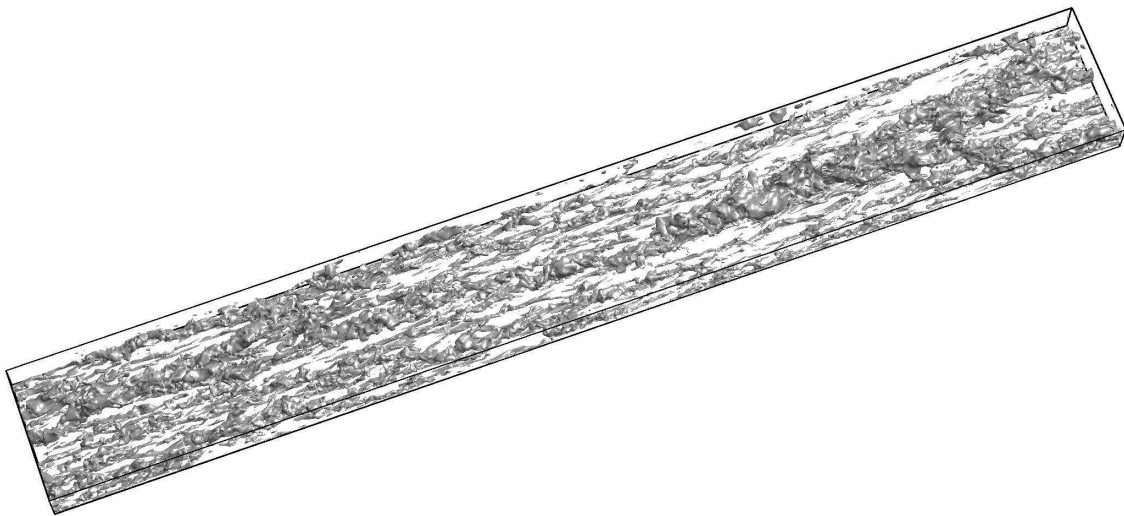

Figure 5. Isosurface of the streamwise fluctuation velocity, $u^+ = -2$, in a computational channel with $h^+ = 550$ [2]. The flow is from left to right, and the box shows the full semi-channel height, and the full periodic streamwise length of the computational box, $25h$. Only a narrow strip of width $3.15h$ is shown. Figure courtesy of O. Flores.
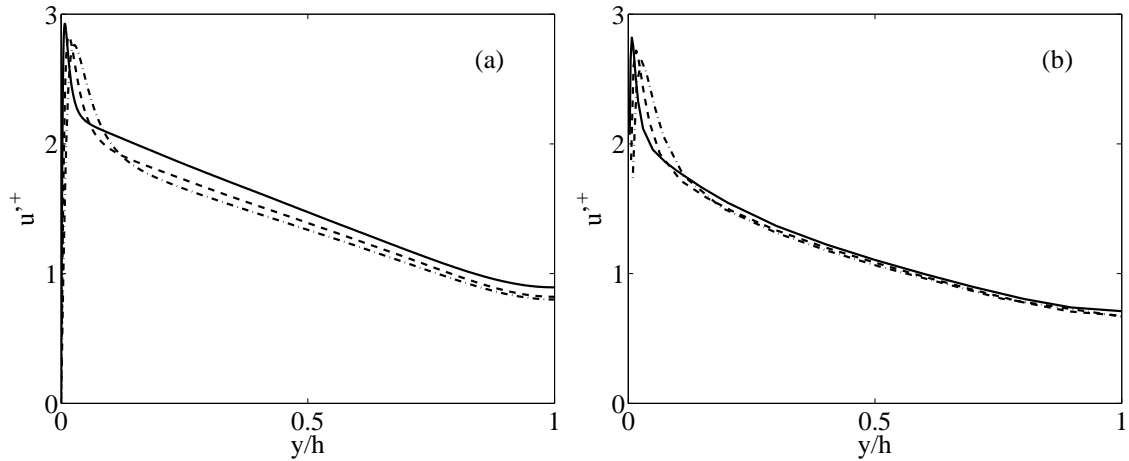
Figure 6. Root-mean-square intensity of the fluctuations of the streamwise velocity in channels at different Reynolds numbers. Data and symbols as in figure 3. (a) Full velocity fluctuations. (b) With the energy removed for structures longer than $\lambda_x = 6h$, and wider than $\lambda_z = h$.

Simple linearized analysis of a uniform shear shows that the long-time asymptotic state of any localized perturbation is a u-streak, but it provides no wavelength-selection mechanism. Viscosity provides a length scale, and the mean profile of real shear flows determines a wall-normal modal structure. The key modelling assumption appears to be to use the same y-dependent eddy viscosity required to maintain the experimental mean profile [44]. Note that this implies that the resulting model applies to averaged eddies, rather than to individual structures. The analysis can be found in [3]. It turns out that there are two sets of wavelengths for which the total energy is most amplified, with eigenfunctions that are localized at the two locations where the viscosity does not depend on y. Near the wall, where the viscosity is mostly molecular, they have spanwise wavelengths and eigenfunctions similar to the observed sublayer streaks. Near the central plane, where $\nu_T \approx u_\tau h$ is also roughly uniform, they are large-scale streaks with spanwise wavelengths of the order of the observed $3h$, and wall-normal eigenfunctions that agree well with the dominant proper orthogonal decomposition eigenmodes of the streamwise velocity at those wavelengths.

We know less about how the ejections are created, but linear analysis also gives some information on them. Although the linear transient growth of the streamwise velocity is by now well established, it is less often realized that, in the same way that transverse perturbations create u-streaks, any u perturbation that is not infinitely long can transfer energy into the transverse velocity components. In fact, the same transient-growth analysis giving the large-scale streaks contains nontrivial amplifications for v and w. This would in principle provide the possibility of a linear cycle in which v ejections create streaks by extracting energy from the mean shear, while the streaks in turn create ejections. Unfortunately the wavelengths that are most amplified for u are not the same ones that are most amplified for v. The former are streaks elongated along x, while the most amplified v and w are roughly isotropic in the wall-parallel plane. This agrees with the spectral evidence in figure 4, but means that nonlinearity would be required to match the wavelengths, and to close the cycle. It is however easy to visualize a process by which an ejection creates a strong streak, whose enveloping shear layer becomes unstable and creates new, shorter ejections. In fact, we have seen that compact ejections can be identified at all scales in the logarithmic and outer layers, both numerically and experimentally, and that they are associated with streaks. It is known, from the analysis of their relative lengths and lifetimes, that the observed ejections cannot be the origin of the full length of the streak to which they are associated, and that some causal link from streaks to ejections is also required [3].

The scenario just described is mostly derived from simulations, and from the linear analysis of the averaged equations of motion. A different scenario has been proposed from the observation of streamwise

sections of experimental flow fields. In it, the basic object is a hairpin vortex growing from the wall, whose induced velocity creates the low momentum ramps mentioned above [1]. In the model, which was motivated by the behaviour of hairpin vortices in the numerical simulation of a particular laminar velocity profile [63], the hairpins regenerate each other, creating vortex packets that are responsible for the very long observed streaks [11]. While the two models look very different at first sight, they can probably be reconciled to a large extent. Vortex packets would correspond to the instability waves on the shear layer around the streak, and the strengthening of the streak by the vortices would correspond to the vortex regeneration process. In fact, preliminary analysis of the averaged flow field in the neighbourhood of ejections suggests that, while the primary streak instability near the wall is sinuous, the dominant modes away from the wall may be varicose, leading in the mean to symmetric hairpins. Varicose perturbations to model streaks have been studied less often than sinuous ones, because the observations of the sublayer streaks clearly suggest a sinuous instability, but, whenever both symmetries have been studied in the same setting, their instability eigenvalues have usually turned out to be of the same order [29].

The main difference between the two models is their respective emphasis on vortices and eddies, although that might be largely a matter of notation, perhaps influenced by the coarser resolution of most experiments when compared with simulations. An apparently more serious difference is the treatment of the effect of the wall. The 'numerical' model emphasizes the effect of the local velocity shear, rather than the presence of the wall, while the 'experimental' one appears to require the formation of the hairpins in the buffer region. That could again be a matter of notation, but it is more likely due to the reliance of the experimental model on laminar numerical simulations, using molecular viscosity [63]. There is little question that large structures in turbulence feel the effect of smaller ones [44]. While the modelling of this randomizing effect as a simple eddy viscosity can be criticized, that model should be much closer to reality than the much weaker molecular dissipation of a laminar environment. When the linear evolution of an initially compact ejection is analysed using the eddy viscosity mentioned above, the structures created near the wall do not grow very much, and most ejections observed at a given wall distance have to be created 'locally' [5]. Indeed, numerical experiments in which the viscous wall cycle is artificially removed have outer-flow ejections and streaks that are essentially identical to those above smooth walls [14]. Experimentally, this is equivalent to the classical observation that the outer layers in turbulent boundary layers are independent of wall roughness [21].

At wall distances between the inner and the outer layers, linear analysis does not provide a single dominant most-amplified wavelength, because the eddy viscosity has no single absolute length scale. The analysis of the initial value problem in that region results in self-similar structures that grow linearly with time. This, however, is probably the most interesting part of the flow, because self-similarity is the most characteristic feature of turbulence, and because the logarithmic layer is the only part of wall-bounded turbulence with the potential of supporting an indefinitely large scale ratio. Whether the linearized equations can say something about this region, or whether nonlinearity is required at all levels, can only be speculated at the moment.

4.1   The logarithmic velocity profile

Before leaving completely the subject of the logarithmic layer, it might be of interest to spend a few paragraphs on the question of the logarithmic velocity profile in (4). That equation was one of the first quantitative theoretical results obtained in turbulence, and it was a genuine prediction. It is difficult to distinguish empirically a power law with a small exponent from a logarithm, and the early engineering correlations for the experimental mean velocities in boundary layers and pipes used power laws, with exponents in the range $0.15 - 0.2$. On the other hand, power laws are theoretically difficult to justify, because dimensional analysis shows that an equation of the type

$$U = \text{Const.}\, y^{\xi}, \tag{5}$$

either requires a characteristic scale for both the velocity and the length, or alternatively none at all. We have seen that u_{τ} acts as a uniform velocity scale in wall-bounded flows, but it is unclear whether (5) should

be written, in the intermediate region, in terms of the viscous length scale, or of the flow thickness. The logarithmic law was formulated as a velocity profile that could be expressed in terms of any length scale. While there have been many derivations, most of them are equivalent to the observation that, if there is no available length scale, the only dimensionally possible form for the mean velocity gradient is

$$\frac{\partial U}{\partial y} = \frac{u_\tau}{\kappa y},$$
(6)

from where (4) follows by integration. The argument is usually credited to Millikan [37], who actually used the requirement that an inner solution, scaled on the viscous length, should match over a finite range of y another solution scaling on the flow thickness. Since the ratio h^+ between the two length scales is arbitrary, this implies that the expression for the velocity profile should work for any length scale, and leads to (6). In fact, the argument has to be slightly more involved, as is easily seen by repeating (6) with the gradient of U^2 substituted for the gradient of U.

Reference [40] recasts the previous argument in terms of the Lie analysis of the invariances of the equations of motion, and notes that the solutions have to be invariant to all the possible transformations. The argument above uses the invariance of the inviscid equations to geometric stretching, which is why it can say nothing about the choice of the dependent variable, but it is only after adding the Galilean invariance, which applies only to U, that (6) is selected. When that is taken into account, the mean velocity can be written as

$$U^+ = \widetilde{U}(y/L) + a(L),$$
(7)

which should be independent of the arbitrary length scale L. Differentiating with respect to L now gives (6). This argument is much closer to Millikan's [37], who matched an inner solution of the form $U_{in}^+(y^+)$, to an outer one expressed in 'defect' form, $U_{centre}^+ - U_{out}^+(y/h)$. The extra additive constant in the defect form is required for the argument.

Note that Galilean invariance makes the logarithmic profile (4) incompatible with the no-slip boundary condition at the wall, but that the logarithm is singular at that point, and that the inviscid equations used to derive it do not, in any case, support tangential boundary conditions.

The question of the detailed derivation of the logarithmic profile is of more than academic interest, and it is striking that even today, almost eighty years after it was originally proposed by Prandtl and Von Kármán, the validity of (4) keeps being regularly challenged, both experimentally and theoretically. A summary of its early history can be found in the book by Schlichting [48]. A flavour of the current controversies, that centre on questions such as whether a scale-independent region really exist, or on which origin should be used for y in (4), can be found in [62, 8, 61].

The main interest of the subject is however that there are variables other than the mean velocity that also show an apparent logarithmic behaviour. Two examples, the fluctuations of the spanwise velocity and of the pressure, are given in figure 7. The figure also includes an example that does not behave logarithmically, for comparison. Logarithmic variables are interesting because they are potentially singular. The increment of such a variable across the logarithmic layer is $O(\log h^+)$, and, in the limit of high Reynolds numbers, it should grow without bound. For none of the two fluctuations plotted in figure 7 can we use Galilean invariance to justify a logarithmic law, and it would be very interesting to understand why these particular variables, and not others, behave in that way. There is also the question of what is actually the law being represented in the figure. It is unclear, for example, whether p', p'^2, or some other power behave logarithmically. The exponent can be varied within fairly wide limits without changing the quality of the fit.

5 Conclusions

We have briefly reviewed the present state of the understanding of the different regions of wall-bounded turbulent flows. The dynamics of the viscous layers near smooth walls is a subject that, like most others
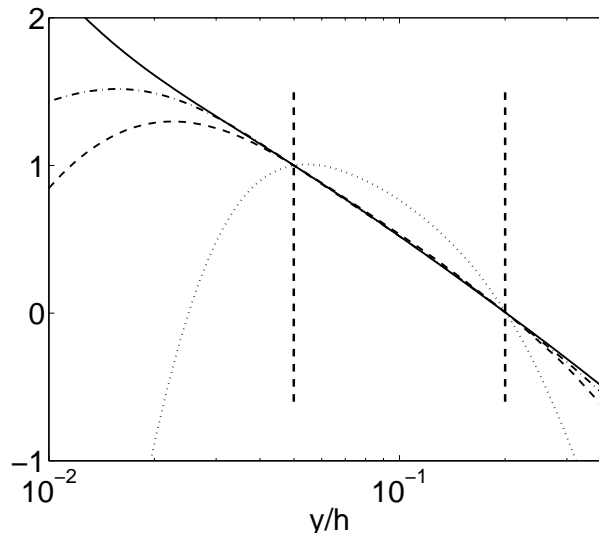
Figure 7. Profiles in a turbulent channel with $h^+ = 2000$ [18] of: ——— , mean velocity; ———— , r.m.s. spanwise velocity; —·— , r.m.s. pressure; ········ , r.m.s. wall-normal velocity. The two vertical lines are $y^+ = 100$ and $y/h = 0.2$, and all curves have been scaled so as to be one and zero at those two limits.

in turbulence, is not completely closed, but which has evolved in the last two decades from empirical observations to relatively coherent theoretical models. It is also one of the first cases in turbulence, perhaps together with the structure of small-scale vorticity in isotropic turbulence, in which the key technique for cracking the problem has been the numerical simulation of the flow. The reason is that the Reynolds numbers of the important structures are low, and therefore accessible to computation, while experiments are difficult. For example the spanwise Reynolds number of the streaks is only of the order of $z^+ = 100$, which is less than a millimetre in most experiments, but we have seen that it is well predicted by the range of parameters in which the associated equilibrium solutions exist. We have seen that the larger structures coming from the outside flow interfere only weakly with the near-wall region, because the local dynamics are intense enough to be always dominant. The spacing of the streaks just mentioned has been observed up to the highest Reynolds numbers of the atmospheric boundary layer [34].

The structures in the viscous layers have a well-defined length scale, determined by viscosity, that allows them to be described as individual objects. In the outer layer, where the relevant length scale is the flow thickness, we have seen that at least some of the structural properties can be described by the linear analysis of the most amplified transient modes of the mean velocity profile. In this case there is however a full turbulent cascade, instead of a single scale, and the eddies can only be described in a statistical sense. The next few years will probably be dominated by modelling efforts for the logarithmic layer, where there is no unique dominant length scale, and where self-similarly growing statistical objects should probably substitute individual structures or modes.

In the opinion of the present author, a key contributor to further progress in this area should be numerical simulation, in the same way as it was for the viscous layers, and for motivating the analysis of the outer ones. The main obstacle at present is one of cost, and was shared by the original low-Reynolds number simulations that eventually led to the understanding of the buffer layer. The simulation in [18] took six months on 2000 supercomputer processors. It took a similar time, twenty years before, to run the simulation in [32] at $h^+ = 180$. As long as each numerical experiment takes such long times, it is only possible to observe the results, and the simulations are little more than better-instrumented laboratory experiments.

As computers improve, however, other things become possible. When the low-Reynolds number simu-

lations of the 1980s became roughly 100 times cheaper in the 1990s, it became possible to experiment with them in ways that were not possible in the laboratory. The series of 'conceptual' simulations that led to the results in section 3 were of this kind.

The cost of simulating the logarithmic layer is beginning to be within the reach of modern computers. The next decade will bring it down to the level at which conceptual dynamical experiments become commonplace. The motivation will be both theoretical and technological. The momentum cascade across the range of scales in the logarithmic layer will probably be the first three-dimensional self-similar cascade to become accessible to computational experiments. Its simplifying feature is the alignment of most of the net transfer along the direction normal to the wall. The main practical drive is probably large-eddy simulation, in which the momentum transfer across scales in the inertial range has to be modelled for the method to be practical [25].

References

[1] Adrian, R. J., Meinhart, C. D. and Tomkins, C. D., (2000). Vortex organization in the outer region of the turbulent boundary layer, *J. Fluid Mech.*, **422**, 1–54.

[2] del Álamo, J. C. and Jiménez, J., (2003). Spectra of very large anisotropic scales in turbulent channels, *Phys. Fluids*, **15**, L41–L44.

[3] del Álamo, J. C. and Jiménez, J., (2006). Linear energy amplification in turbulent channels, *J. Fluid Mech.*, **559**, 205–213.

[4] del Álamo, J. C., Jiménez, J., Zandonade, P. and Moser, R. D., (2004). Scaling of the energy spectra of turbulent channels, *J. Fluid Mech.*, **500**, 135–144.

[5] del Álamo, J. C., Jiménez, J., Zandonade, P. and Moser, R. D., (2006). Self-similar vortex clusters in the logarithmic region, *J. Fluid Mech.*, **561**, 329–358.

[6] Aubry, N., Holmes, P., Lumley, J. L. and Stone, E., (1988). The dynamics of coherent structures in the wall region of a turbulent boundary layer, *J. Fluid Mech.*, **192**, 115–173.

[7] Bakewell, H. P. and Lumley, J. L., (1967). Viscous sublayer and adjacent wall region in turbulent pipe flow, *Phys. Fluids*, **10**, 1880–1889.

[8] Barenblatt, G. I., Chorin, A. J. and Prostokishin, V. M., (2000). Self-similar intermediate structures in turbulent boundary layers at large Reynolds numbers, *J. Fluid Mech.*, **410**, 263–283.

[9] Brown, G. and Roshko, A., (1974). On the density effects and large structure in turbulent mixing layers, *J. Fluid Mech.*, **64**, 775–816.

[10] Butler, K. M. and Farrell, B. F., (1992). Three-dimensional optimal perturbations in viscous shear flow, *Phys. Fluids A*, **4**, 1637–1650.

[11] Christensen, K. T. and Adrian, R. J., (2001). Statistical evidence of hairpin vortex packets in wall turbulence, *J. Fluid Mech.*, **431**, 433–443.

[12] Darcy, H., (1854). Recherches expérimentales rélatives au mouvement de l'eau dans les tuyeaux, *Mém. Savants Etrang. Acad. Sci. Paris*, **17**, 1–268.

[13] DeGraaf, D. B. and Eaton, J. K., (2000). Reynolds number scaling of the flat-plate turbulent boundary layer, *J. Fluid Mech.*, **422**, 319–346.

[14] Flores, O. and Jiménez, J., (2006). Effect of wall-boundary disturbances on turbulent channel flows, *J. Fluid Mech.*, **566**, 357–376.

[15] Gustavsson, L. H., (1991). Energy growth of three-dimensional disturbances in plane Poiseuille flow, *J. Fluid Mech.*, **224**, 241–260.

[16] Hagen, G. H. L., (1839). Über den Bewegung des Wassers in engen cylindrischen Röhren, *Poggendorfs Ann. Physik Chemie*, **46**, 423–442.

[17] Hamilton, J. M., Kim, J. and Waleffe, F., (1995). Regeneration mechanisms of near-wall turbulence structures, *J. Fluid Mech.*, **287**, 317–248.

[18] Hoyas, S. and Jiménez, J., (2006). Scaling of the velocity fluctuations in turbulent channels up to $Re_\tau = 2003$, *Phys. Fluids*, **18**, 011702.

[19] Hutchins, N. and Marusic, I., (2007). Evidence of very long meandering features in the logarithmic region of turbulent boundary layers, *J. Fluid Mech.*, **579**, 467–477.

[20] Jiménez, J., (1998). The largest scales of turbulence, in *CTR Ann. Res. Briefs*, Stanford Univ., 137–154.

[21] Jiménez, J., (2004). Turbulent flows over rough walls, *Ann. Rev. Fluid Mech.*, **36**, 173–196.

[22] Jiménez, J., del Álamo, J. C. and Flores, O., (2004). The large-scale dynamics of near-wall turbulence, *J. Fluid Mech.*, **505**, 179–199.

[23] Jiménez, J., Kawahara, G., Simens, M. P., Nagata, M. and Shiba, M., (2005). Characterization of near-wall turbulence in terms of equilibrium and 'bursting' solutions, *Phys. Fluids*, **17**, 015105.

[24] Jiménez, J. and Moin, P., (1991). The minimal flow unit in near-wall turbulence, *J. Fluid Mech.*, **225**, 221–240.

[25] Jiménez, J. and Moser, R. D., (2000). LES: where are we and what can we expect?, *AIAA J.*, **38**, 605–612.

[26] Jiménez, J. and Pinelli, A., (1999). The autonomous cycle of near wall turbulence, *J. Fluid Mech.*, **389**, 335–359.

[27] Jiménez, J. and Simens, M. P., (2001). Low-dimensional dynamics in a turbulent wall flow, *J. Fluid Mech.*, **435**, 81–91.

[28] Jiménez, J. and Wray, A. A., (1998). On the characteristic of vortex filaments in isotropic turbulence, *J. Fluid Mech.*, **373**, 255–285.

[29] Kawahara, G., Jiménez, J., Uhlmann, M. and Pinelli, A., (2003). Linear instability of a corrugated vortex sheet – a model for streak instability, *J. Fluid Mech.*, **483**, 315–342.

[30] Kawahara, G. and Kida, S., (2001). Periodic motion embedded in plane Couette turbulence: regeneration cycle and burst, *J. Fluid Mech.*, **449**, 291–300.

[31] Kim, H. T., Kline, S. J. and Reynolds, W. C., (1971). The production of turbulence near a smooth wall in a turbulent boundary layer, *J. Fluid Mech.*, **50**, 133–160.

[32] Kim, J., Moin, P. and Moser, R. D., (1987). Turbulence statistics in fully developed channel flow at low Reynolds number, *J. Fluid Mech.*, **177**, 133–166.

[33] Kim, K. and Adrian, R. J., (1999). Very large-scale motion in the outer layer, *Phys. Fluids*, **11**, 417–422.

[34] Klewicki, J. C., Metzger, M. M., Kelner, E. and Thurlow, E., (1995). Viscous sublayer flow visualizations at $R_\theta \approx 1,500,000$, *Phys. Fluids*, **7**, 857–863.

[35] Kolmogorov, A. N., (1941). The local structure of turbulence in incompressible viscous fluids a very large Reynolds numbers, *Dokl. Akad. Nauk. SSSR*, **30**, 301–305. Reprinted in *Proc. R. Soc. London.* A, **434**, 9–13 (1991).

[36] Meinhart, C. D. and Adrian, R. J., (1995). On the existence of uniform momentum zones in a turbulent boundary layer, *Phys. Fluids*, **7**, 694–696.

[37] Millikan, C. B., (1938). A critical discussion of turbulent flows in channels and circular tubes, in *Proc. 5th Intl. Conf. on Applied Mechanics*, Wiley, 386–392.

[38] Morrison, W. R. B., Bullock, K. J. and Kronauer, R. E., (1971). Experimental evidence of waves in the sublayer, *J. Fluid Mech.*, **47**, 639–656.

[39] Nagata, M., (1990). Three-dimensional finite-amplitude solutions in plane Couette flow: bifurcation from infinity, *J. Fluid Mech.*, **217**, 519–527.

[40] Oberlack, M., (2001). A unified approach for symmetries in plane parallel turbulent shear flows, *J. Fluid Mech.*, **427**, 299–328.

[41] Österlund, J. M., Johansson, A. V., Nagib, H. M. and Hites, M., (2000). A note on the overlap region in turbulent boundary layers, *Phys. Fluids*, **12**, 1–4.

[42] Reddy, S. C., Schmid, P. J., Baggett, J. S. and Henningson, D. S., (1998). On stability of streamwise streaks and transition thresholds in plane channel flows, *J. Fluid Mech.*, **365**, 269–303.

[43] Reddy, S. C., Schmid, P. J. and Henningson, D. S., (1993). Pseudospectra of the Orr–Sommerfeld operator, *SIAM J. App. Math.*, **53**, 15–47.

[44] Reynolds, W. C. and Hussain, A. K. M. F., (1972). The mechanics of an organized wave in turbulent shear flow. Part 3. Theoretical models and comparisons with experiments, *J. Fluid Mech.*, **54**, 263–288.

[45] Reynolds, W. C. and Tiederman, W. G., (1967). Stability of turbulent channel flow, with application to Malkus' theory, *J. Fluid Mech.*, **27**, 253–272.

[46] Richardson, L. F., (1920). The supply of energy from and to atmospheric eddies, *Proc. Roy. Soc. A*, **97**, 354–373.

[47] Robinson, S. K., (1991). Coherent motions in the turbulent boundary layer, *Ann. Rev. Fluid Mech.*, **23**, 601–639.

[48] Schlichting, H., (1968). *Boundary layer theory*, McGraw-Hill, sixth edition.

[49] Schoppa, W. and Hussain, F., (2002). Coherent structure generation in near-wall turbulence, *J. Fluid Mech.*, **453**, 57–108.

[50] Sirovich, L. and Zhou, X., (1994). Dynamical model of wall-bounded turbulence, *Phys. Rev. Lett.*, **72**, 340–343.

[51] Smith, C. R. and Metzler, S. P., (1983). The characteristics of low speed streaks in the near wall region of a turbulent boundary layer, *J. Fluid Mech.*, **129**, 27–54.

[52] Swearingen, J. D. and Blackwelder, R. F., (1987). The growth and breakdown of streamwise vortices in the presence of a wall, *J. Fluid Mech.*, **182**, 255–290.

[53] Tennekes, H. and Lumley, J. L., (1972). *A first course in turbulence*, MIT Press.

[54] Toh, S. and Itano, T., (2001). On the regeneration mechanism of turbulence in the channel flow, in *Proc. Iutam Symp. on Geometry and Statistics of Turbulence*, editors T. Kambe, N. T. and T. Muiyauchi, Kluwer, 305–310.

[55] Toh, S. and Itano, T., (2003). A periodic-like solution in channel flow, *J. Fluid Mech.*, **481**, 67–76.

[56] Townsend, A., (1976). *The structure of turbulent shear flow*, Cambridge U. Press, second edition.

[57] Waleffe, F., (1997). On a self-sustaining process in shear flows, *Phys. Fluids*, **9**, 883–900.

[58] Waleffe, F., (1998). Three-dimensional coherent states in plane shear flows, *Phys. Rev. Lett.*, **81**, 4140–4143.

[59] Waleffe, F., (2001). Exact coherent structures in channel flow, *J. Fluid Mech.*, **435**, 93–102.

[60] Waleffe, F., (2003). Homotopy of exact coherent structures in plane shear flows, *Phys. Fluids*, **15**, 1517–1534.

[61] Wosnik, M., Castillo, L. and George, W. K., (2000). A theory for turbulent pipe and channel flows, *J. Fluid Mech.*, **421**, 115–145.

[62] Zagarola, M. V., Perry, A. E. and Smits, A. J. (1997). Log laws or power laws: The scaling of the overlap region, *Phys. Fluids*, **9**, 2094–2100.

[63] Zhou, J., Adrian, R. J. S. B. and Kendall, T. M. (1999). Mechanisms for generating coherent packets of hairpin vortices in channel flow, *J. Fluid Mech.*, **387**, 353–396.

Javier Jiménez
School of Aeronautics
Universidad Politécnica
28040 Madrid, Spain
and Centre for Turbulence Research
Stanford University, Stanford CA, 94305 USA
`jimenez@torroja.dmt.upm.es`